Acta Geochim
https://doi.org/10.1007/s11631-024-00735-w

ORIGINAL ARTICLE

Experimental studies on CO_2 sequestration via enhanced rock weathering in seawater: Insights for climate change mitigation strategies in coastal and open ocean environments

Arshad Ali[1,2] · Muhammad I. Kakar[3] · Mohamed A. K. El-Ghali[1,4] · Hafiz Ur Rehman[5] · Iftikhar A. Abbasi[4] · Mohamed Moustafa[4]

Received: 10 January 2024 / Revised: 29 August 2024 / Accepted: 1 September 2024

Abstract Enhanced weathering (EW) of ultramafic rocks from the Muslim Bagh Ophiolite, Pakistan, has been studied in laboratory experiments to explore carbon sequestration as a climate change mitigation strategy for coastal and open sea environments. The research focused on a cost-effective ex situ experiment to examine the effects of EW reaction pathways arising from the interactions among rock powder, seawater and CO_2. The experimental filtrates from different milled peridotite samples exhibit a decrease in the Mg/Ca ratio as the specific surface area increases, which accelerates reaction rates. This suggests that the leached Mg from the original rock may have been consumed in the formation of brucite, serpentine and carbonates during EW. Similar reaction pathways are also responsible for the chemical alterations observed in amphibolite, albeit to varying degrees. On the other hand, the experimental residues showed an increase in loss on ignition compared to the original rock, indicating that EW has facilitated the incorporation of H_2O and CO_2 into secondary mineral structures through various reaction pathways, leading to the formation of brucite, serpentine and carbonates. Thermal gravimetric analysis of the experimental residues confirms the presence of these minerals based on their decomposition temperatures. Additionally, XRD analysis identified a range of carbonates in the residues of both peridotite and amphibolite samples, validating the occurrence of carbonation reactions. SEM images reveal textural changes in both samples, supporting the formation of secondary minerals through EW, consistent with observations from the petrographic study of untreated samples. Control experiments on CO_2 absorption in seawater showed a decrease in pH, highlighting ocean acidification from increased CO_2 emissions. However, when rock powder was added to the seawater-CO_2 mixture, the pH increased. This suggests that the EW of ultramafic rock powders can sequester CO_2 while raising seawater pH through the formation of secondary minerals. This research could serve as an analog for EW applications, considering the worldwide abundance of ultramafic rocks and the availability of coastal and open ocean environments. However, further research is required to understand the behavior of other elements and

Supplementary Information The online version contains supplementary material available at https://doi.org/10.1007/s11631-024-00735-w.

✉ Arshad Ali
arshadali@squ.edu.om

Muhammad I. Kakar
kakarmi.cemuob@gmail.com

Mohamed A. K. El-Ghali
melghali@squ.edu.om

Hafiz Ur Rehman
hafiz@sci.kagoshima-u.ac.jp

Iftikhar A. Abbasi
iftikhar@squ.edu.om

Mohamed Moustafa
m.moustafa@squ.edu.om

[1] Earth Sciences Research Centre, Sultan Qaboos University, Al Khoudh, Muscat, Oman

[2] UNESCO Chair on Ophiolite Studies, Sultan Qaboos University, Al Khoudh, Muscat, Oman

[3] Center of Excellence in Mineralogy, University of Balochistan, Quetta, Pakistan

[4] Department of Earth Sciences, Sultan Qaboos University, Al Khoudh, Muscat, Oman

[5] Department of Earth and Environmental Sciences, Kagoshima University, Kagoshima City, Japan

Published online: 18 September 2024

their impacts on ocean chemistry in EW processes before applying CO_2 sequestration strategies.

Keywords CO_2 sequestration · Ocean acidification · Coastal enhanced weathering · Muslim Bagh Ophiolite · Carbon mineralization · Peridotite

1 Introduction

Since the industrial revolution, the extensive use of fossil fuels has disturbed the carbon dioxide (CO_2) emission-sink balance, resulting in excessive greenhouse gas emissions, particularly CO_2, which contributes to global warming (Betts et al. 2023). The Intergovernmental Panel on Climate Change (IPCC) set a goal of limiting global warming to < 2 °C above pre-industrial levels, and 197 countries pledged to meet that goal in the Paris Agreement 2015 (UNFCCC 2015). In 2022, it is estimated that anthropogenic activities such as fossil fuel combustion, deforestation, cement production and land-use changes released approximately 40.7 ± 3.2 Gt of CO_2 into the atmosphere (Friedlingstein et al. 2023). The amount of CO_2 released by human activity is only half of what is still in the atmosphere. In March 2024, the annual average atmospheric CO_2 concentration touched 425 ppm, exceeding the pre-industrial level by nearly 150 ppm, as reported by NASA (https://climate.nasa.gov/vital-signs/carbon-dioxide/?intent=121).

Numerous strategies have been proposed to achieve these ambitious goals, with geological carbon storage in ultramafic rocks emerging as a prominent solution in many mitigation frameworks aimed at reducing atmospheric CO_2 levels (Sanna et al. 2014; Mark et al. 2010; Zhu et al. 2016; Fawzy et al. 2020). This requires the direct industrial carbonation of calcium- and magnesium-rich silicate minerals, such as olivine, pyroxene and serpentine, under elevated pressure and temperature conditions, referred to as *ex-situ* and *in-situ* carbonation methods. Suitable rock formations for this process include mafic rocks like basalt and gabbro as well as ultramafic rocks like peridotite (e.g., Gerdemann et al. 2007; Jia and Anthony 2002; O'Connor et al. 2005; Kelemen and Matter 2008; Sanna et al. 2014). Peridotite, an ultramafic rock type, is distinguished by its mineral makeup, which includes > 40% olivine along with pyroxenes such as orthopyroxene and clinopyroxene. This composition can be found in harzburgite, wehrlite and lherzolite, which include > 40% olivine in addition to pyroxene. Dunite, another type of peridotite, is differentiated by its composition of > 90% olivine and < 10% pyroxene (Streckeisen 1976).

It is commonly found as residual mantle peridotite exposed on the seafloor and in ophiolites. When ophiolitic peridotite undergoes hydration and carbonation, the resulting reaction products such as serpentine, talc, magnesite, dolomite and calcite exhibit higher Mg values than the olivine and pyroxene reactants. Essentially, an ophiolite represents oceanic crust exposed on land. For example, the Samail Ophiolite in Oman and the United Arab Emirates (UAE) in the Arabian Peninsula has the largest block of peridotite on Earth's surface, with about 15,000 km^3 of peridotite within a few kilometers of depth (Nicolas et al. 2000; Kelemen and Matter 2008). This makes it a site with significant mineral carbonation potential, capable of storing 30 trillion tons of CO_2 (Matter and Kelemen 2009). Oman is located on the southeastern coast of the Arabian Peninsula, sharing borders with the UAE, Saudi Arabia and Yemen. It also has coastlines along the Arabian Sea and the Gulf of Oman.

Recently, it is observed that approximately 80 % of the carbon in the calcite sample, formed following the alteration of peridotite from the Samail Ophiolite, is attributed to atmospheric CO_2, based on modeling using the carbon and oxygen isotope system (Ali et al. 2021). With 68 ophiolite and numerous basaltic units scattered across the globe, carbon mineralization, a natural process where CO_2 reacts with minerals to form stable carbonates, is emerging as a promising method for CO_2 removal and sequestration, offering a potential solution to mitigate global warming. To date, two important pilot projects have been successfully completed: the CarbFix project in Iceland (Matter et al. 2016) and the Wallulla Basalt project in the US (McGrail et al. 2017, 2014, 2011). The process of injecting CO_2 into mafic and ultramafic rocks, known as *in-situ* carbonation, aims to convert the injected CO_2 gas into carbonate rock through reactions with the host rock, for example, as demonstrated by carbonation of olivine-rich rocks in Oman (Kelemen and Matter 2008). According to these authors, it is estimated that annually up to 1 billion tons of CO_2 could potentially be injected into these rocks in Oman. However, the transportation of such large volumes of CO_2 from industries and coal-fired power plants in the industrialized world, as well as the purification and delivery to a remote site, poses a significant logistical challenge. The necessary handling and transportation make this solution far from economical. However, CO_2 injected into the basalt of the CarbFix site in Iceland, demonstrating that the long-term storage of anthropogenic CO_2 emissions through mineralization can occur much more rapidly than previously thought. Most of the injected CO_2 was mineralized in less than 2 years (Matter et al. 2016).

Contrarily, one of the ex situ approaches involves crushing the rocks to a fine grain size (Gerdemann et al. 2002, 2007; Kakizawa et al. 2001; Kojima et al. 1997; O'Connor et al. 2000) and subjecting them to temperatures ranging from 100 to 185 °C and CO_2 partial pressures of 4 to 15 MPa (Gerdemann et al. 2007). However, such treatments incur significant energy consumption and costs (Huijgen et al. 2006). Another method involves pretreating the crushed rocks with acid to extract Ca^{2+}, Mg^{2+} and Fe^{2+} ions (Goff

and Lackner 1998; Haywood et al. 2001; Kakizawa et al. 2001), but this alternative is less favorable because of its high acid consumption (Haywood et al. 2001).

The idea of applying enhanced weathering specifically in coastal areas likely gained traction as researchers sought innovative methods to address the challenges of rising CO_2 levels and ocean acidification. This constitutes the primary operational method for both land-based and aquatic applications. The mineral grains undergo chemical weathering, wherein they dissolve and consequently capture CO_2 directly from the atmosphere in terrestrial applications or enhance CO_2 uptake from the aqueous medium by elevating water alkalinity or proton consumption (Montserrat et al. 2017) in coastal and open ocean applications. Since May 2022, Vesta (vesta.earth), a US-based company, has been carrying out such projects in various US states such as Massachusetts (Herring River), New York (Long Island) and North Carolina (Duck) in collaboration with various academic institutions for wetland restoration and blue carbon, beach nourishment and nearshore placement. Another nearshore placement project is planned for July 2024 in South Carolina (Jeremy Cay).

The ocean has proven to be an effective atmospheric CO_2 sink by being able to absorb about 9.5 billion tons of CO_2 annually between 1800 and 1994 (Friedlingstein et al. 2023; Watson et al. 2020; Gruber et al. 2019; Le Quéré et al. 2015). The ocean is currently undergoing a significant change in its chemistry known as "ocean acidification" (OA), which results in an increase in dissolved inorganic carbon (DIC) and bicarbonate ions as well as a decrease in the pH and carbonate ion (CO_3^{2-}) concentrations of seawater (Orr et al. 2005). The marine ecosystem is also impacted by OA because it depends on specific carbonate chemistry parameters to survive (IPCC 2021; Riebesell et al. 2013; Gatusso and Hansson 2011). The strategies for carbon dioxide removal (CDR) that have been investigated to mitigate OA are enhanced weathering (EW) or ocean alkalinity enhancement (OAE), a carbon capture technology that involves increasing ocean alkalinity by depositing rock particles in the ocean (Kantzas et al. 2022; Beerling et al. 2020, 2018; Fuss et al. 2018; Renforth et al. 2015; Hartmann et al. 2013; Schuiling and Krijgsman 2006). To mitigate the effects of OA on the marine ecosystem, it is suggested that both EW and OAE can be implemented (Taylor et al. 2016). It is simple to implement this strategy in coastal and open ocean areas with agricultural lands that provide additional benefits like higher crop yields and the prevention of soil erosion (Beerling et al. 2018; Dietzen et al. 2018; Köhler et al. 2010). In general, EW and OAE are potential OA and global warming mitigation strategies by lowering atmospheric CO_2 via carbonate formation for long-term secure storage (Gattuso et al. 2015; Doney et al. 2009). Globally, there is a guarantee of the supply of essential mineral resources, especially olivine, for the storage of carbon. This is especially true in Oman and Pakistan, which have coastlines of 3165 and 1365 km^2, respectively, enabling coastal and open ocean applications. Sandy beaches are the major component of these coastlines, serving as buffer zones to protect the coast from marine attack and erosion. Beaches may lose sand during storms and subsequently regain it during calms, resulting in an equilibrium. Yet, addressing erosion issues, which vary in intensity, necessitates prompt implementation of sustainable management strategies (Pilkey and Cooper 2004; Al-Hartushi et al. 2014). The ongoing rise in sea levels and the likely intensification of extreme events could make circumstances in coastal areas especially sandy shores worse, according to the Intergovernmental Panel on Climate Change (IPCC) Fifth Assessment Report (Tignor and Allen 2013). These changes are linked to stresses imposed by humans and global warming caused by the use of fossil fuels (IPCC 2013). According to optical satellite images taken since 1984, 31 % of the world's ice-free coastline is sandy. Data also show that 24 % of the world's sandy beaches are degrading at rates > 0.5 m/year, 28 % are accreting, and 48 % are stable (Luijendijk et al. 2018). The bulk of the sandy shoreline in marine protected zones is degrading, which raises serious concerns. From 1984 to 2015, roughly 28 000 km^2 of the world's coastline experienced erosion, which is approximately twice the area that was formed through accumulation processes (Mentaschi et al. 2018). Given that beach erosion can act as a catalyst for the widespread use of large amounts of crushed olivine in coastal areas, where it can do two things: (1) help reduce coastal erosion and (2) naturally absorb CO_2.

In this study, we explored the application of coastal and open ocean enhanced weathering using ultramafic rocks sourced from the Muslim Bagh Ophiolite (MBO) in Balochistan, Pakistan. These rocks are notable for their abundance of magnesium-rich minerals, such as olivine and pyroxene, found in mylonitic peridotite (MP3), as well as magnesium- and calcium-rich minerals like amphibole present in amphibolite (MP7). Choosing these rocks is essential as magnesium oxide (MgO) proves highly effective in carbon sequestration, needing only 3.4 tons of MgO to capture the CO_2 equivalent of 1 ton of carbon, whereas 4.7 tons of calcium oxide (CaO) are necessary (Lackner et al. 1995).

2 Experimental and analytical methods

2.1 Samples

Two samples were collected from the Muslim Bagh Ophiolite (MBO) in Balochistan, Pakistan, to conduct a comparative analysis of the impacts of enhanced weathering on the chemical composition of ultramafic rocks with distinct

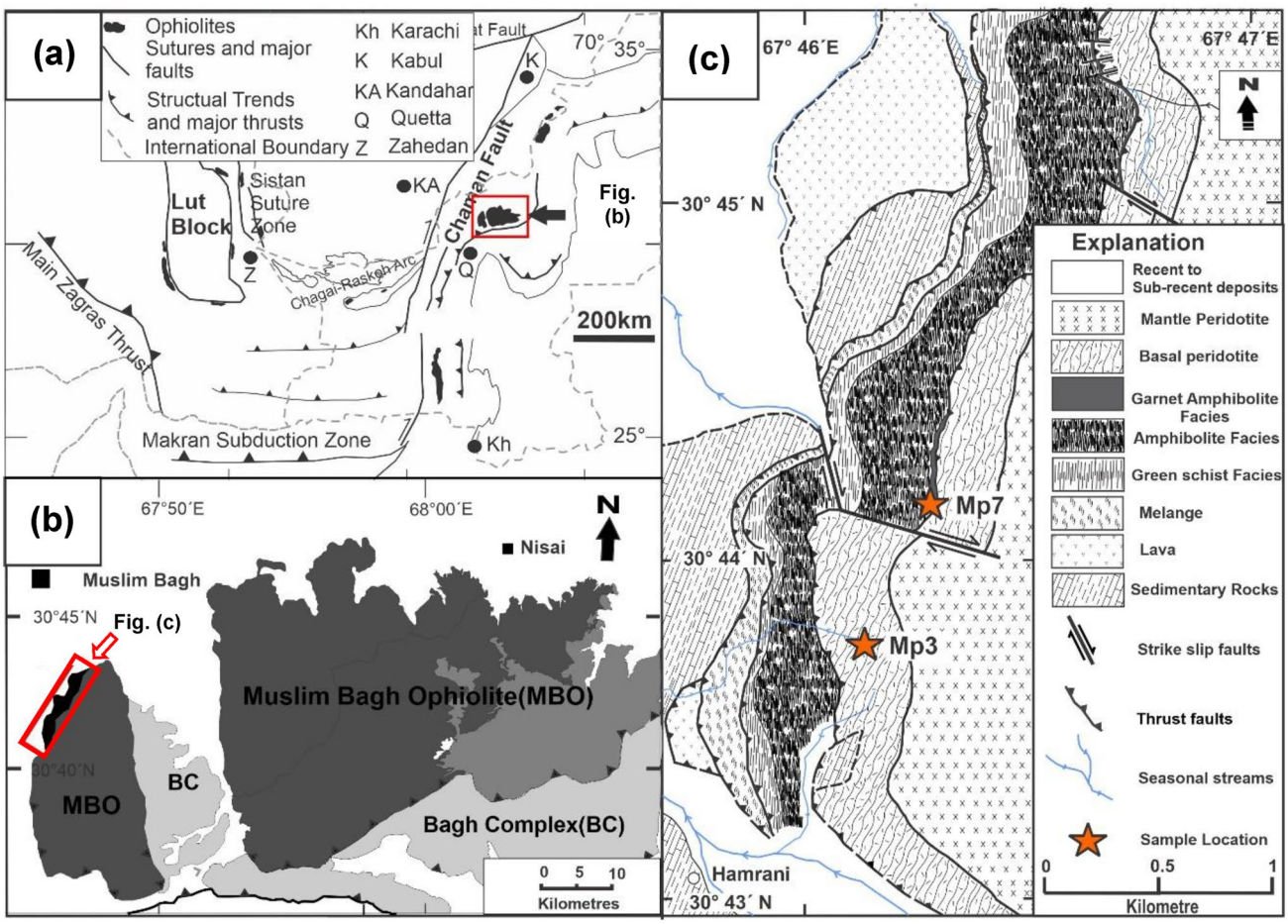

Fig. 1 A regional geological map illustrating an ophiolite formation, suture zones and fault lines, including international boundaries (**a**). A geological map of the Muslim Bagh Ophiolite (MBO) in Balochistan, Pakistan (**b**). A modified geological map depicting different rock units and the locations of collected samples within the MBO (**c**; Kakar et al. 2014)

mineralogy (Fig. 1). Sample MP3 is a mylonitic peridotite (coordinates: latitude: 30.7165116; longitude: 67.7724118) with major minerals such as forsterite (Mg_2SiO_4) and enstatite ($MgSiO_3$), and sample MP7 is an amphibolite with major minerals such as tremolite [$Ca_2Mg_5Si_8O_{22}(OH)_2$] and albite ($NaAlSi_3O_8$) (Fig. 2). Calcite forms the observed white crust on the sample MP7 (Fig. 2d). Seawater was collected from the Seeb Beach in Oman (23°41′43.7″ N, 58°09′27.9″ E). Thin sections of both samples were prepared and examined at Kagoshima University in Japan to determine their petrographic features (see Results section for details).

2.2 Experimental setup and analytical methods

The experimental setup for conducting enhanced weathering was designed around three components of the starting reaction material (Fig. 3). Component 1 represents seawater collected from Seeb Beach in Oman, which was filtered using Whatman® filter paper (hardened 50) to retain fine crystalline residue prior to pH testing (Fig. 3a). The filtered saltwater was tested for alkali and alkaline earth metals such as Na (14 300 ppm), K (491 ppm), Mg (1600 ppm) and Ca (430 ppm) at ALS Arabia Biyaq-Oman, using the ICP-OES technique. Component 2 includes rock powders obtained from two distinct samples (MP3, MP7), which were used to form slurries with seawater (Fig. 3b). The rocks were ground into powders using a HERZOG miller (HSM 100H) to perform ball milling. The procedure was carried out within a tungsten carbide vessel to prevent potential contamination attributable to the hardness of the rocks. During the milling process, intermittent breaks were introduced every 10 min to prevent overheating of the sample. Ball milling was conducted for each sample for a total duration of 90 min, excluding the intermittent breaks. During the milling process, specific amounts of the milled sample were collected at 30-min intervals to obtain powders with varying surface areas. The estimated specific surface areas of the powders

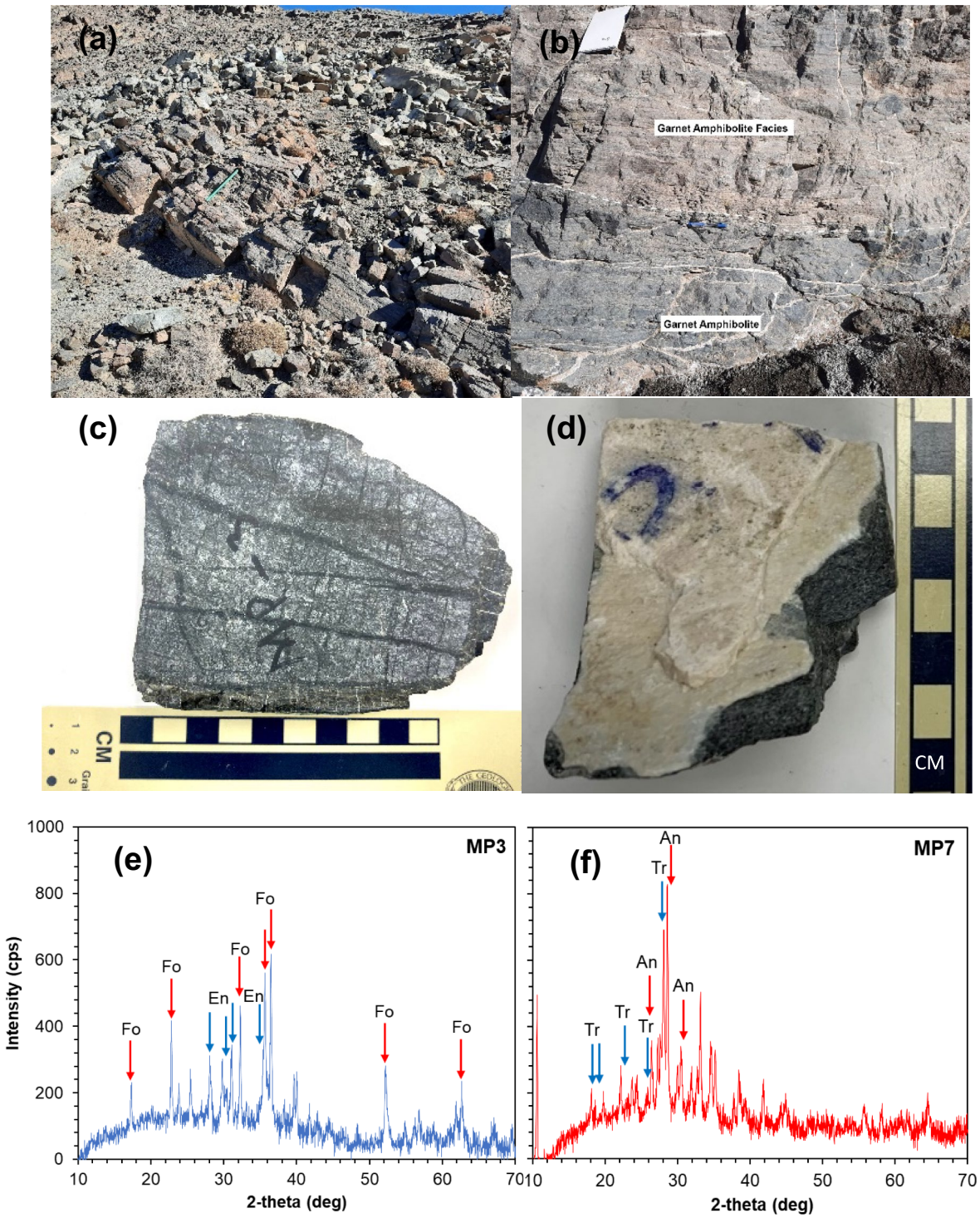

Fig. 2 (**a**, **c**). Images of the outcrops and hand specimens of mylonitic peridotite (MP3) and (**b**, **d**) amphibolite (MP7) from the metamorphic sole rocks of Muslim Bagh Ophiolite in Balochistan, Pakistan. The sample MP7 exhibits a white crust that is composed of calcite (**d**). Mineral identification by XRD reveals that the main mineral phases are forsterite (Fo) and enstatite (En) in MP3 (**e**) and tremolite (Tr) and anorthite (An) in MP7 (**f**)

milled for 30, 60 and 90 min are 14, 24 and 28 m^2/g, respectively, based on the BET curve provided in a previous study (Rigopoulos et al. 2018; see Fig. 1). Component 3 involved the construction of a pressurized CO_2 source via the use of a soft drink (Fig. 3c). Initially, a 225-mL bottle was used as a container for extracting CO_2 from the soft drink. This

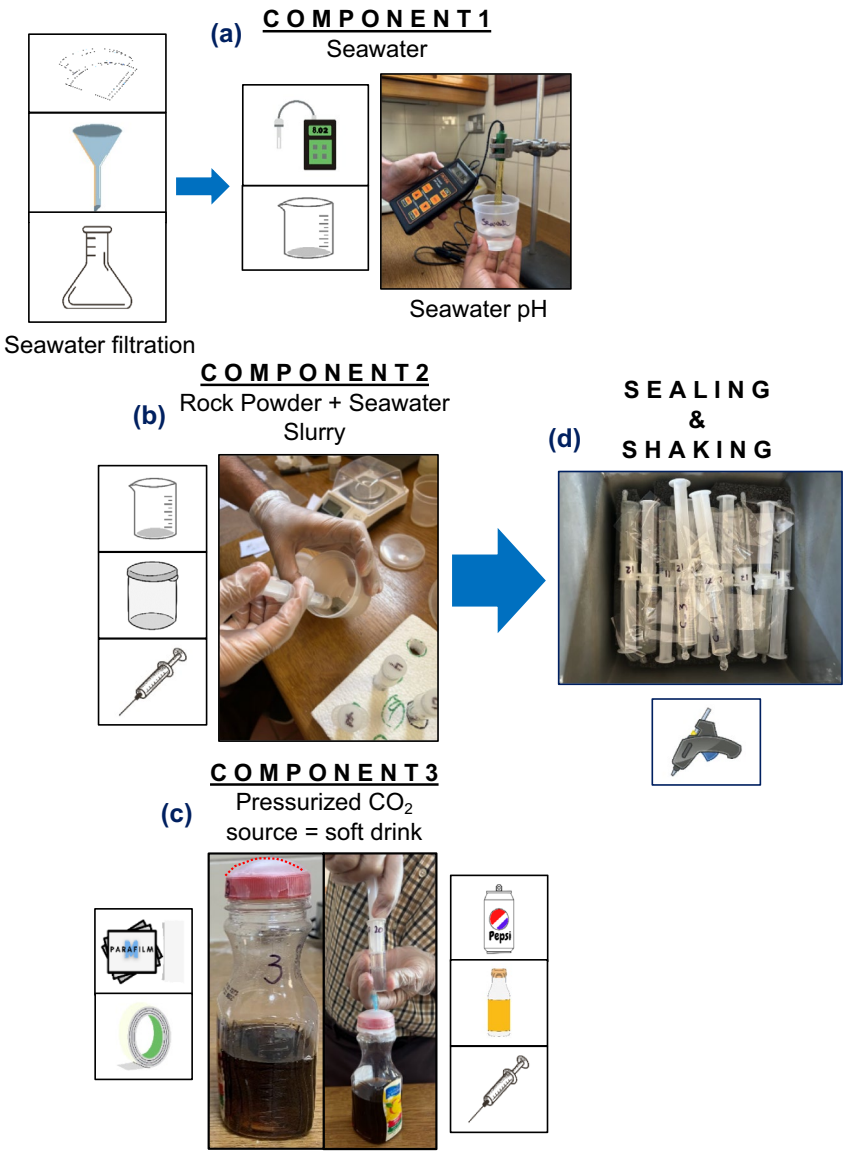

Fig. 3 An illustration of the experimental setup showing the three starting materials used in the enhanced weathering experiments: seawater (**a**), rock powder (**b**) and carbon dioxide source (**c**). The mixture was put into a 10-mL syringe, sealed and left to react for 130 days with periodic shaking (**d**)

was accomplished by creating a hole with a diameter of 2.5 cm in the bottle cap and sealing it with layers of parafilm. This setup made it possible to use a medical syringe with a sharp needle to extract CO_2 gas from the bottle's headspace. A clean bottle was filled with 100 mL of the soft drink; subsequently, the cap was sealed with adhesive tape to prevent the CO_2 gas present in the head space from leaking. The beverage was carefully shaken for 30 s to extract the CO_2 gas into the head space, and then the bottle was left to stand for another 2 to 3 min. Then, a sharp needle was used to transfer the CO_2 (4 mL of the gas with a concentration of 735 ± 55 ppm of CO_2 gas) into a reaction syringe that held the sample slurry (Fig. 3c). The protocols for estimating the CO_2 concentration injected into the reaction syringe are described in the supplementary information. Finally, the reaction syringes were sealed, and the components were mixed and agitated for an average of 8 h each day during working hours, excluding weekends, over a period of 130 days (Fig. 3d). The experimental mixture was filtered, and the residues were then subjected to x-ray diffractometer (XRD), scanning electron microscopy (SEM) and thermogravimetric analysis (TGA) to determine their mineral and chemical compositions.

2.2.1 X-ray diffraction (XRD)

X-ray diffraction (XRD) analyses were carried out at the Earth Sciences Research Centre, Sultan Qaboos University, using a benchtop MiniFlex600 diffractometer manufactured by Rigaku. The instrument was configured with a copper (Cu) target tube and a detector (SC) and operated at 40 kV and 15 mA. Before the analysis, the samples were finely ground using an agate mortar and pestle. Then, block samples were prepared on an aluminum sample plate to be

exposed to Cu Kα radiation, with a scanning speed set at 2.5° 2θ•min^{-1}. The resulting diffraction data were processed using PDXL basic software to determine peak characteristics such as position, height, integrated intensity and full width at half maximum (FWHM). The identification of mineral phases was carried out using a licensed database (PDF-4 Minerals, 2023) provided by the International Center for Diffraction Data (ICDD®).

2.2.2 Scanning electron microscopy (SEM)

Scanning electron microscopy (SEM) was used to get images of two selected samples, MP3 and MP7, at the Surface Laboratory within the College of Science at Sultan Qaboos University. The powdered samples were fixed to a standard aluminum SEM stub using carbon paint. Furthermore, a thin layer of platinum was deposited as a coating to facilitate the imaging of surface morphologies. The SEM analysis was done utilizing a field emission SEM (JEOL JSM-7600F, Japan) operating at 15 kV.

2.2.3 X-ray fluorescence (XRF)

Major element analyses were conducted at the Central Analytical and Applied Research Unit (CAARU), Sultan Qaboos University, using a sequential wavelength dispersive x-ray fluorescence (WDXRF) spectrometer. This spectrometer, equipped with a rhodium (Rh) target x-ray tube, was operated at exciting voltages of 25 kV and current of 160 mA. Prior to preparing the fused beads for XRF analysis, powdered samples (3 g) were ignited in ceramic crucibles at 850 °C for 2 h to determine the loss on ignition (LOI; Table S1). LOI is a common technique used to assess various properties of geological samples, including water content, organic , inorganic carbon and other volatile elements. For the fused beads, a 0.5 g portion of the powdered sample was mixed with 10 g of lithium borate flux in a platinum crucible and heated to 1000 to 1200 °C to produce a homogeneous glass disc. The SuperQ 5.3A software was used for spectrometer control and sample measurement, covering elements from sodium (Na) to uranium (U) and concentrations ranging from parts per million (ppm) to high percentages.

2.2.4 Thermogravimetric analysis (TGA)

Experiments on the decomposition characteristics of the samples were conducted using a PerkinElmer Pyris Series—TGA 4000 thermogravimetric analyzer at Qatar University. The furnace was heated from 30 to 995 °C at a rate of 10 °C/min. The gas flow, comprising oxygen, was set at 20 mL/min. The sample's weight was continuously monitored as a function of temperature.

2.2.5 Inductively coupled plasma-optical emission spectroscopy (ICP-OES)

The analysis of seawater and experimental filtrates was done by the ALS Arabia Biyaq-Oman using ICP-OES technique following the methods of USEPA (1994).

3 Results

3.1 Mineral characterization and petrography

The mylonitic peridotite (MP3), mainly composed of olivine (e.g., forsterite) and pyroxene (e.g., enstatite) and amphibolite (MP7), has amphibole (e.g., tremolite) and plagioclase (e.g., albite) as the main phases along with a white calcite layer on the surface (Fig. 2d). For the study of EW and OAE, minerals rich in magnesium (Mg), calcium (Ca) and iron (Fe) play critical role by supplying the necessary divalent ions required for the carbonate formation process. For example, chlorite envelops the olivine and is positioned between the olivine and serpentine in sample MP3 as shown in PPL and XPL photomicrographs (Fig. 4a, b). It is important to observe a minor calcite vein in the images (Fig. 4a, b). During serpentinization, olivine reacts with water to form serpentine, which is a group of minerals having fibrous or scaly structures and is characterized by its green color (Fig. 4b). This reaction can be written as follows (Eq. 1):

$$\begin{aligned}&\text{Olivine } (Mg_2SiO_4) + \text{Water}(H_2O) \rightarrow \text{Serpentine}[Mg_3Si_2O_5(OH)_4]\\&+ \text{Chlorite } [Mg_5Al_2Si_3O_{10}(OH)_8]\end{aligned} \quad (1)$$

3.2 Chemical characterization

MP3 and MP7 both contain minerals rich in Mg, Ca and Fe, such as forsterite, enstatite and tremolite (Fig. 2e, f). Analysis of the XRD data reveals that the MP3 sample exhibits a substantially greater abundance of forsterite, comprising over two-thirds of the enstatite content. These mineral compositions led to the selection of these samples for enhanced weathering experiments as they can release divalent ions of Mg, Ca and Fe, which can react with carbonate and bicarbonate species in seawater to form carbonates. Following the EW experiment, notable texture variations in the experimental residues and the untreated samples are evident (Fig. 5). The untreated MP3 and MP7 powders exhibited distinct alterations in surface morphologies following the EW experiments, implying the occurrence of a chemical reaction (Fig. 5 a, f). Furthermore, the LOI and TGA data

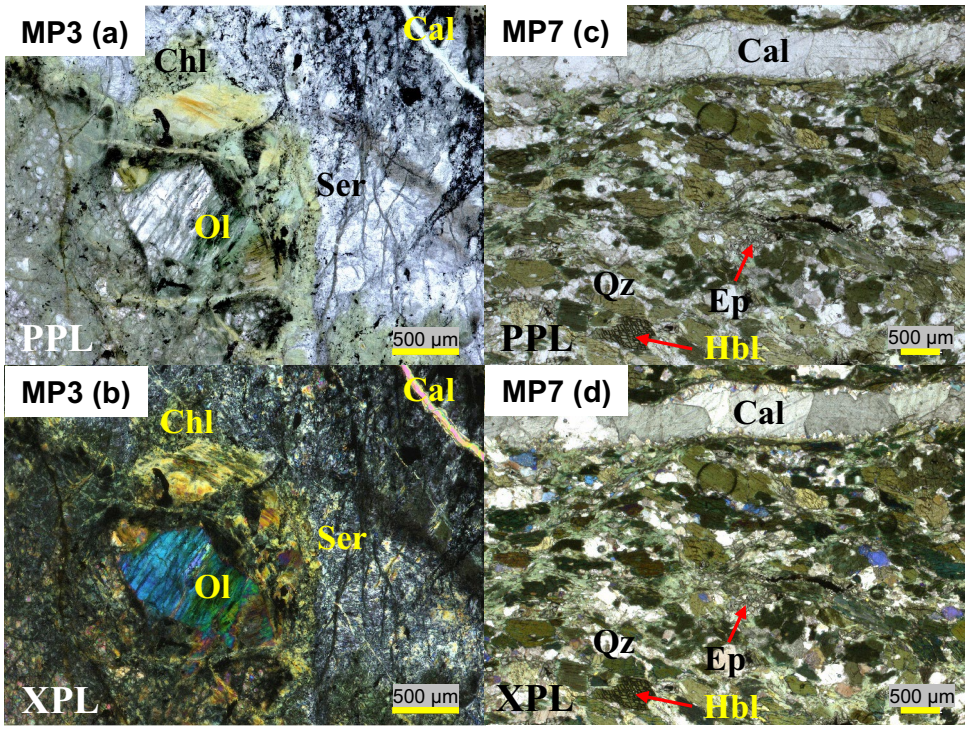

Fig. 4 Microphotographs of MP3 (**a.** PPL, **b.** XPL) and MP7 (**c.** PPL, **d.** XPL). The MP3 shows olivine surrounded by chlorite, which is sandwiched between olivine and serpentine. Hornblende and epidote can be seen alongside quartz in MP7. Note that calcite veins can be seen in both samples. Abbreviations: *PPL* plane-polarized light, *XPL* cross-polarized light, *Chl* chlorite, *Cal* calcite, *Ep* epidote, *Hbl* hornblende, *Ol* olivine, *Qz* quartz, *Ser* serpentine

reveal a significant change in mass loss of the residues compared to the untreated samples (Figs. 6, 7). The LOI includes the release of H_2O and CO_2 from various minerals formed during the EW process, including brucite, serpentine and carbonates (Figs. 6, 7).

The pH value of the filtrate obtained from MP3-30 is higher at 8.77 compared to those of the filtrates from MP3-60 and MP3-90, which measure 8.60 and 8.58, respectively. In contrast, when compared to the initial pH of the original seawater (8.04), the pH of the MP7 filtrates increases (MP7-30 = 8.50; MP7-60 = 8.34; MP7-90 = 8.52) but remains relatively similar within the range of uncertainty. However, when observing multiple runs of control filtrates, there is a noticeable decrease in pH from 8.04 to the range of 7.50–7.80 (Fig. 8).

4 Discussion

4.1 Control filtrates

Like in the ocean, carbon dioxide in the reaction syringe is expected to exist in three distinct inorganic forms: as free carbon dioxide, $CO_{2(aq)}$ (aqueous carbon dioxide), as bicarbonate, HCO_3^- and as carbonate ion, CO_3^{2-}. A fourth form, carbonic acid (H_2CO_3), exists, but its concentration is typically much lower than that of $CO_{2(aq)}$ (Eq. 2). The combined concentration of the two electrically neutral forms, H_2CO_3 and $CO_{2(aq)}$, which are chemically inseparable, is commonly represented as CO_2 or H_2CO_3. When CO_2 reacts with seawater to form H_2CO_3, the concentration of hydrogen ions (H+) increases (Eq. 2; Zeebe and Wolf-Gladrow 2001).

$$CO_2(\text{gas}) \leftrightarrow CO_2(\text{aqueous}) + H_2O \leftrightarrow H_2CO_3 \leftrightarrow HCO_3^- + H^+ \leftrightarrow CO_3^{2-} + 2H^+ \quad (2)$$

The elemental compositions of alkali metals (e.g., Na, K) and alkaline earth metals (e.g., Mg, Ca) in seawater are compared with those in the filtrates from control experiments involving CO_2 absorption in seawater (Fig. 9). Following the reaction of seawater with CO_2, the elemental compositions exhibit reductions of 75 % (Na), 76 % (K), 73 % (Mg) and 76 % (Ca), indicating the removal of these metals during the filtration process. It is likely that alkali metals form bicarbonates because Na and K bicarbonates ($NaHCO_3$ and $KHCO_3$) are more stable and less soluble in water than their corresponding carbonates (Tro 2022). The carbonates are highly soluble in water, resulting in a strong alkaline solution containing Na^+ and K^+ ions, as well as CO_3^{2-} ions. This suggests that the reduction of alkali metals in the control filtrates is caused by the formation of bicarbonates in the presence of CO_2 (Fig. 9).

For alkaline metals, $CaCO_3$ is more stable than calcium bicarbonate [$Ca(HCO_3)_2$]. Furthermore, $CaCO_3$ has a low

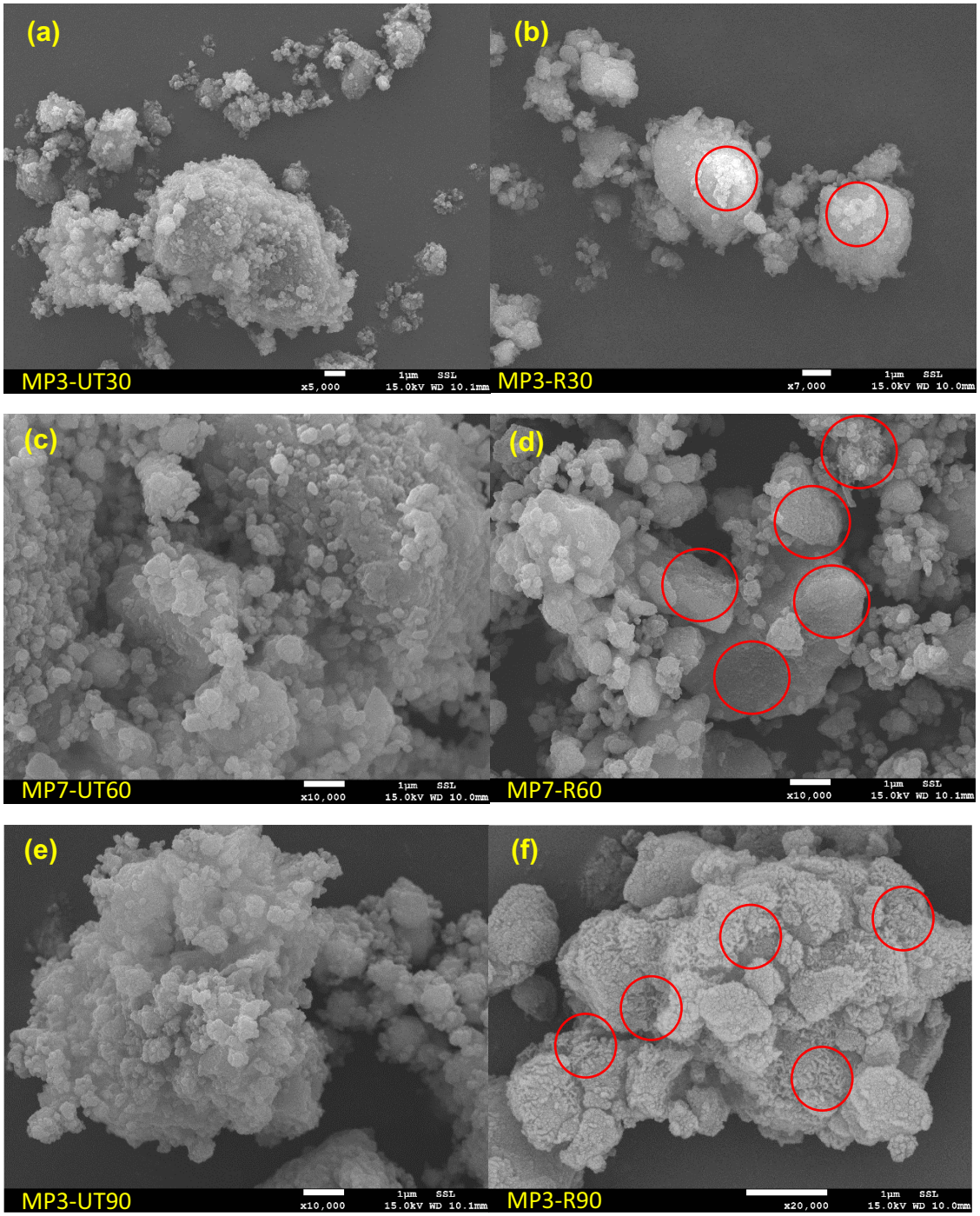

Fig. 5 SEM images reveal textures of untreated (UT) sample powders pulverized for 30, 60 and 90 min (**a**: MP3-UT30; **c**: MP7-UT60; **e**: MP3-UT90). The red circles highlight the morphological alterations, such as the formation of spheroid aggregates of carbonates, occurring on the surfaces of Mg-, Ca- and Fe-bearing minerals in experimental residues (R) (**b**: MP3-R30; **d**: MP7-R60; **f**: MP3-R90)

solubility and only a small amount will dissolve in water, particularly in the presence of CO_2, resulting in a weakly basic solution. Conversely, $[Ca(HCO_3)_2]$ forms when $CaCO_3$ reacts with H_2CO_3 and is relatively less stable than $CaCO_3$ (Tro 2022). Magnesium behaves similarly to calcium under these conditions. This implies that the reduction of alkaline metals in the control filtrates is due to the formation of carbonates in the presence of CO_2 (Fig. 9).

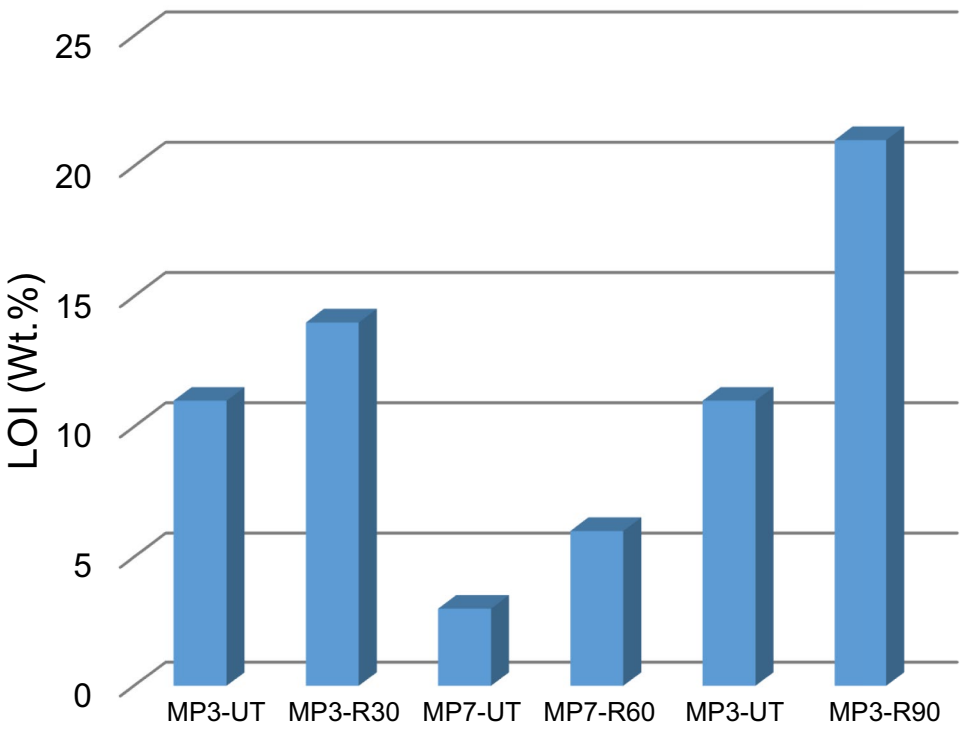

Fig. 6 Plot showing changes in loss on ignition (LOI) before and after the enhanced weathering experiment

4.2 Assessment of pH levels in experimental and control filtrates

In general, atmospheric CO_2 dissolves in seawater, resulting in the formation of H_2CO_3. A similar reaction can be expected within the reaction syringe, where the CO_2 present in the headspace interacts with seawater in the control experiment and with the sample slurry in the reactor during the experimental setup. (Eq. 3).

$$CO_2(gas) + H_2O \rightarrow H_2CO_3 \quad (3)$$

The presence of sufficient CO_2 in the headspace of the reaction syringe causes the formation of H_2CO_3, which lowers the pH of the control runs even though the alkali and alkaline earth metals in seawater produce bicarbonates and carbonates, as discussed above. This reaction increases the concentration of H^+ ions in the seawater, leading to a decrease in pH (Fig. 8). The three plotted pH values for each control run are as follows: (1) the measurement taken after the experiment; (2) the reading after the reaction syringe is gently shaken, which causes a slight pH increase; (3) the reading after vigorous shaking, which causes a further pH increase (Fig. 8). This phenomenon occurs when the temperature rise from shaking causes the seawater to release CO_2, which lowers the carbonic acid content. These findings imply that the production of H_2CO_3 lowers the pH of control runs.

Conversely, the formation of carbonates in seawater can raise the pH of the seawater because of chemical reactions that consume hydrogen ions, thereby making the water more alkaline. The dissolved carbonate minerals in seawater, such as $CaCO_3$, when reacting with H_2CO_3, form HCO_3^- ions.

$$H_2CO_3 + CaCO_3 \rightarrow Ca(HCO_3)_2 \quad (4)$$

$$Ca(HCO_3)_2 + H_2CO_3 \rightarrow 2HCO_3^- + Ca^{(2+)} \quad (5)$$

These reactions result in the removal of H^+ from the solution, causing a decrease in the concentration of H^+ ions in the seawater. Because of the chemical reactions (Eqs. 4–5), the concentration of H^+ ions in the seawater decreases, causing the pH to rise. A higher pH value indicates that the seawater becomes more alkaline. Likewise, in the presence of CO_2, the interaction between seawater and rock powder resulted in a pH rise (Fig. 8). When seawater reacts with rock powder containing minerals rich in Mg and Ca in the presence of CO_2, it enhances the leaching of Mg and Ca ions into the seawater. This, in turn, triggers the formation of bicarbonate and carbonate compounds of Mg and Ca. Consequently, this process leads to the elevation of seawater pH, primarily attributable to the formation of carbonate species.

The pH of the control filtrates varies between 7.50 and 7.90, while for the experimental filtrates, it ranges from 8.30 to 8.50. This indicates that in the control filtrates, the concentrations of the dissolved carbonate species increase in the order of $H_2CO_3 < CO_3^{2-} < CO_2 < HCO_3^-$ at pH 7.5.

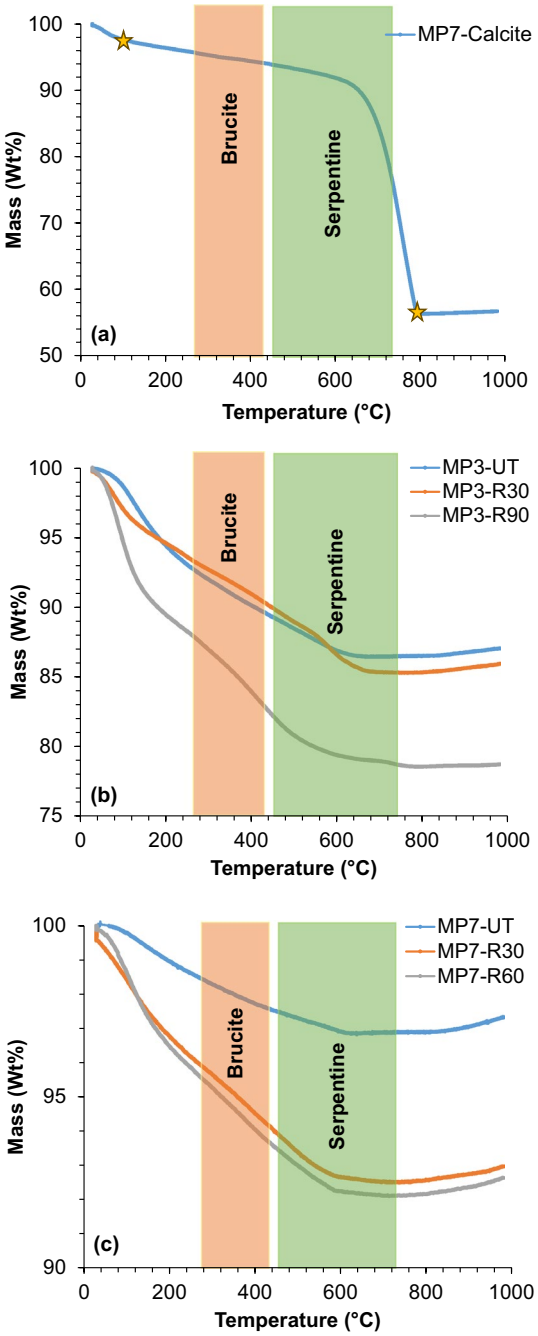

Fig. 7 TGA spectra of MP7 calcite (**a**), untreated sample and experimental residues of MP3 (**b**) and MP7 (**c**). The pink and green shaded areas indicate the decomposition temperature ranges for brucite and serpentine, respectively

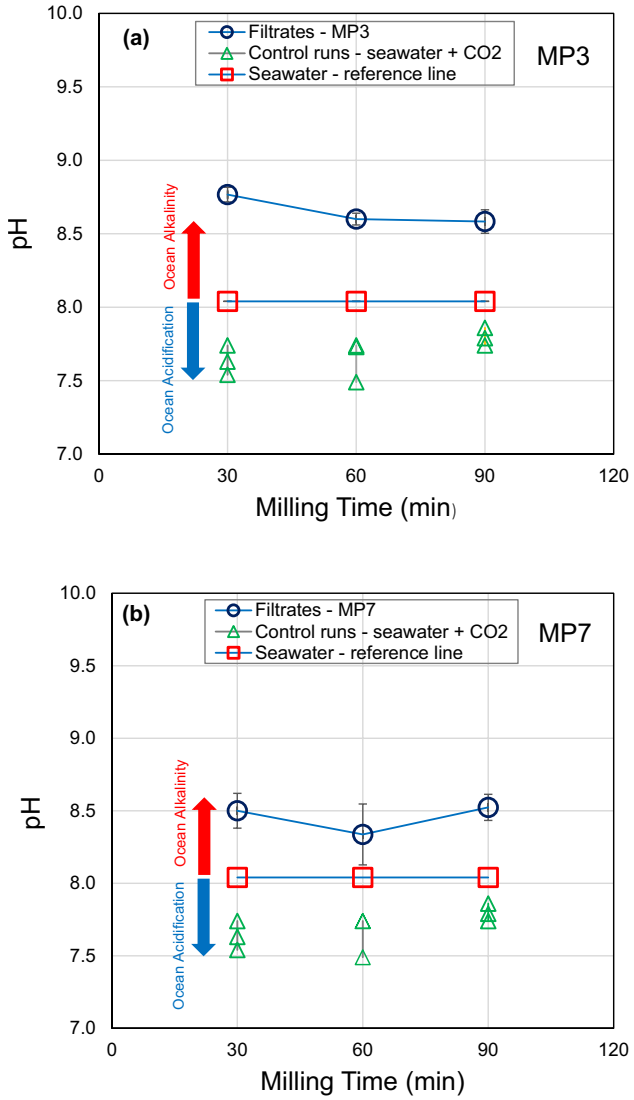

Fig. 8 The pH change in experimental filtrates (circles) obtained from reaction charges of samples milled at 30, 60 and 90 min for MP3 (**a**) and MP7 (**b**). The pH of control runs (i.e., seawater + CO_2; triangles) falls below the original seawater pH (8.04; squares) plotted as a reference line. Note that the pH of control runs is shown for comparison and they are unrelated to milling times. For each run, the three pH values fluctuate as follows: (1) the measurement obtained post-experiment, (2) the reading following a gentle shaking of the reaction syringe resulting in a slight pH increase and (3) subsequently, a further pH increase after vigorous shaking

Conversely, in the experimental filtrates at pH 8.5, the order is $CO_2 < CO_3^{2-} < HCO_3^-$ (Zeebe 1999). The carbonate species that are most dominant in both situations are HCO_3^- and CO_3^{2-}, indicating that these species will produce alkali and alkaline earth metal bicarbonates and carbonates if they have access to Ca and Mg ions. When the pH falls within the range of 7.5 to 8.5, CO_2 speciation occurs according to the following equation (Eq. 6).

$$CO_2 + CO_3^{2-} + H_2O \rightarrow 2HCO_3^- \quad (6)$$

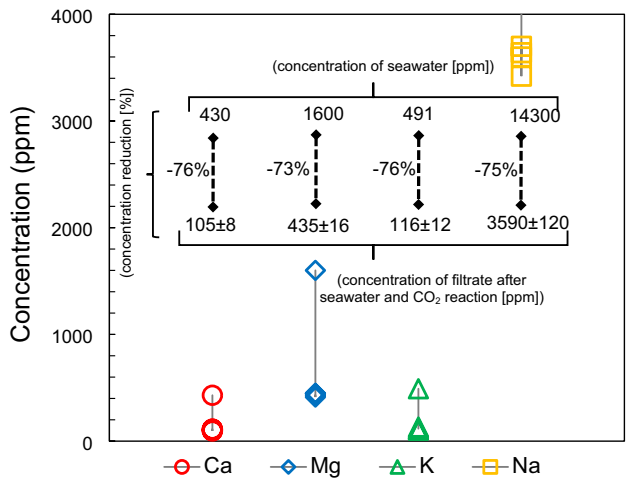

Fig. 9 Comparison of the elemental compositions of seawater before and after CO_2 absorption in control runs. The open symbols (top) attached to the solid lines represent seawater concentrations, while the bottom ones represent compositions of the control filtrates after CO_2 absorption in seawater for 130 days at room temperature. The numerical values indicated by the upper and lower ends of the dashed lines denote the elemental concentrations in seawater and filtrates after CO_2 absorption in the control runs, including percentage reductions in concentration. Filtrate concentrations are given as the average of four separate runs, along with their corresponding standard deviations

4.3 LOI and TGA data

The rise in LOI in residues of MP3 and MP7, milled for different times, compared to their untreated counterparts (Table S1), implies that the reaction among rock, seawater and CO_2 has led to the formation of minerals that contain either H_2O or CO_2 (Fig. 6). Furthermore, the increase in LOI is correlated with an increase in the specific surface area of the rock powder, as demonstrated by the values observed in MP3-30 (14 wt%) and MP3-90 (21 wt%) samples. Previous studies have also shown that the reactivity of Mg-silicates can be significantly enhanced through milling, leading to a reduction in particle size to > 1 μm correlated with increase in the specific surface area (Rigopoulos et al. 2018, 2016a, b, 2015; Turianicová et al. 2013; Huag et al. 2010). The increasing trend in LOI demonstrates a direct correlation with the specific surface area of both samples. The larger surface area promotes more extensive chemical reactions among the components (e.g., rock powder, seawater, CO_2) of the experimental charge, as observed in MP3-30 and MP3-90 (Fig. 6). However, it is unclear which specific chemical reactions involving decomposition are responsible for the increase in LOI (Eqs. 7–9).

$$MCO_3 \rightarrow MO + CO_2(\text{carbonate}) \quad (7)$$

where M = Ca, Mg, Fe etc.

$$Mg(OH)_2 \rightarrow MgO + H_2O\ (\text{brucite}) \quad (8)$$

$$2Mg_3Si_2O_5(OH)_4 \rightarrow 3Mg_2SiO_4 + SiO_2 + 4H_2O(\text{serpentine}) \quad (9)$$

To estimate the contribution of each chemical reaction to the LOI, TGA data are obtained and plotted (Fig. 7). Initially, the calcite separated from the MP7 sample shows a two-step mass loss: 2.37% between 30 and 100 °C and 41.3% between 100 and 800 °C (Fig. 7a). The first step is primarily the loss of physically adsorbed water (drying), while the second step involves the removal of CO_2 (calcination) from the calcite, leaving behind CaO. The main mass loss occurs between 600 and 800 °C, consistent with calcite data, which differs from aragonite and vaterite (Siva et al. 2017). The TGA spectra of untreated MP3 and MP7 samples and their respective experimental residues of various particle sizes are compared in terms of mass loss during heating from 30 to 995 °C at a rate of 10 °C per minute (Fig. 7b, c). Untreated MP3 and MP7 samples exhibit single-step mass losses of 12.9 and 3.2%, respectively, which differ slightly from the LOI values (Table S1). The difference in mineralogy between the two samples suggests that the variations in mass loss observed in LOI and TGA are primarily due to the presence of serpentine and calcite (Fig. 4). Serpentine decomposes at 450–730 °C (Viti 2010), while calcite decomposes at 650–750 °C (Siva et al. 2017). The multistep decomposition of MP3 residues, in contrast to the single-step decomposition of MP7 residues, indicates distinct chemical reactions during EW. MP3-R30 and MP3-R90 residues exhibit mass losses of 14.0 and 21.2% in three and four steps, respectively. For MP3-R30, the mass losses occurred over temperature ranges of 30–270 °C (6.7 %), 270–500 °C (4.4 %) and 500–980 °C (2.9 %). In the case of MP3-R90, the mass losses were observed over temperature ranges of 30–120 °C (7.3 %), 120–270 °C (5.2 %), 270–630 °C (8.2 %) and 630–980 °C (0.53 %). The first step mass loss is likely due to the water adsorbed on the surface of the powder sample. On the other hand, the residues MP7-R30 and MP7-R60 experienced mass losses of 6.85 and 7.36%, respectively, in a single step when heated from 30 to 980 °C (Fig. 7c). Additionally, a slight increase in the mass of both residues after 800 °C is probably indicative of iron oxidation.

To summarize the data, it is evident that EW has generated carbonates, brucite and serpentine, as demonstrated by the chemical reactions above (Eqs. 7–9). The LOI and TGA data indicate that these reactions occur relatively faster with reduced grain size (Fig. 7). The proportion of

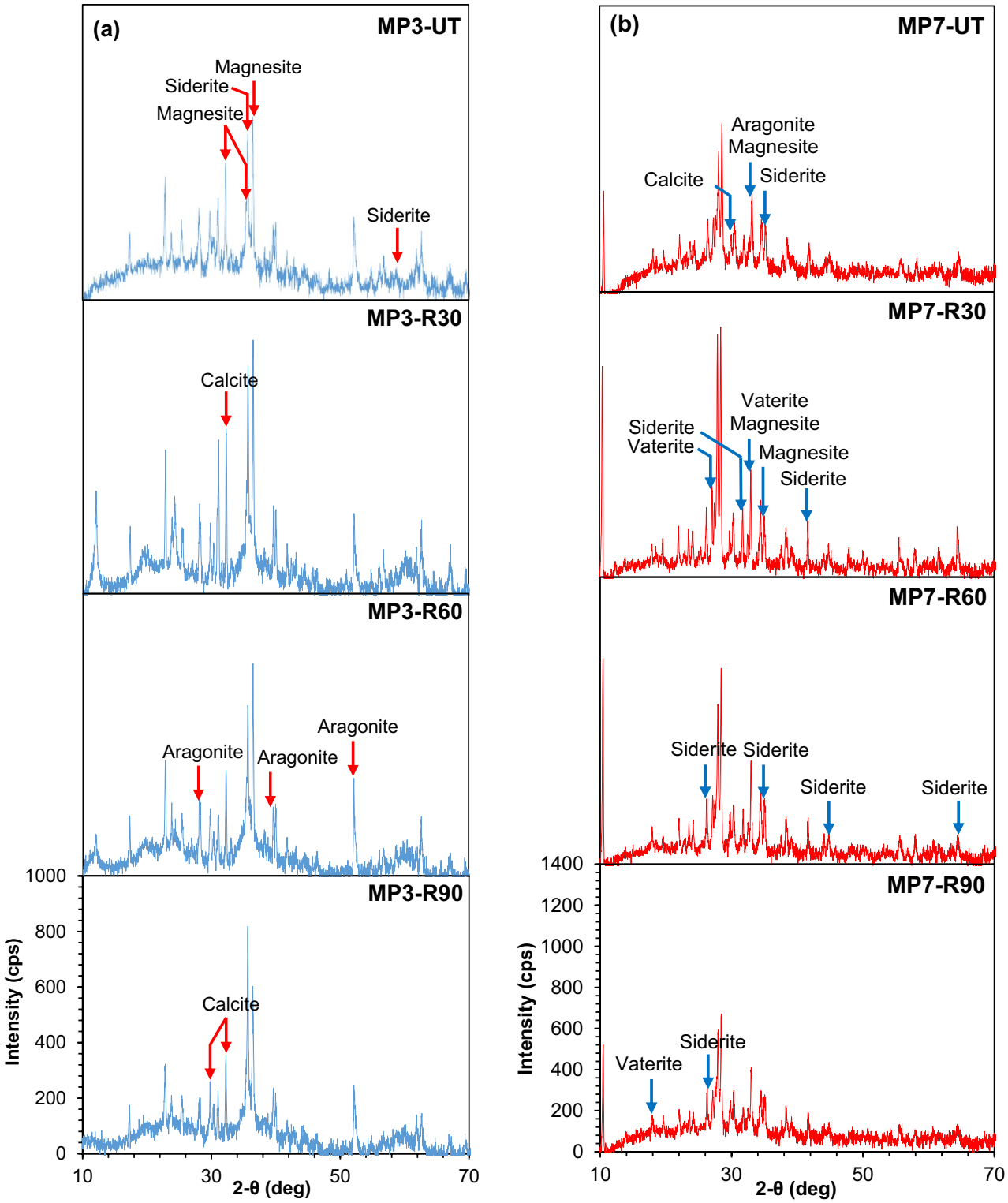

Fig. 10 A comparative XRD spectra illustrates carbonate peaks present in untreated (UT) samples, including MP3-UT (**a**) and MP7-UT (**b**), together with their experimental residues obtained after the EW experiment, which involved the interaction of rock powder and seawater in the presence of CO_2. The suffices added to the sample names denote the milling durations at 30 min (MP3-R30 and MP7-R30), 60 min (MP3-R60 and MP7-R60) and 90 min (MP3-R90 and MP7-R90)

carbonate is lower than that of brucite and serpentine. Thus, further experiments at varying pH and temperature conditions are necessary to understand the preferential carbonate formation.

4.4 Detection of carbonates by XRD

The XRD analysis conducted on both MP3 and MP7 samples, as well as their corresponding residues obtained from powders milled at intervals of 30, 60 and 90 min, revealed the presence of various carbonates containing Ca, Mg and Fe (Fig. 10). The two most common carbonate forms found in MP3 residues are aragonite and calcite (Fig. 10a). Interestingly, the residue of the MP3-60 sample shows a notable preference for the formation of the $CaCO_3$ polymorph aragonite as the primary carbonate species over calcite. This phenomenon could be attributed to the relatively high Mg/Ca ratio (i.e., 21; for major element compositions, see Table S2 in the supplementary information) in MP3-F60 and the experimental temperature range (15–30 °C), as documented in a previous study (see Fig. 1 of Balthasar and Cusack 2015). According to their findings, calcite tends to predominate when the Mg/Ca ratio is < 1, while aragonite becomes prevalent when the ratio is > 2 within the temperature range of 15–30 °C, with a co-precipitation occurring in between. Notably, aragonite emerges as the primary mineral when the Mg/Ca ratio equals 2 at 30 °C, Mg/Ca equals 3 at 20 °C and Mg/Ca exceeds 4 at 15 °C. Conversely, despite MP7 having a Mg/Ca ratio of approximately 16 (Table S2), there is no aragonite formation; instead, MP7-60 is predominantly composed of siderite (Fig. 10b). This inconsistency could be attributed to variations in the mineralogy of the powders, influencing the availability of Mg, Ca and Fe ions for interaction with the carbonate ions available in the reaction syringe. For example, the Mg/Ca ratio indicates that the filtrates from the experimental runs for MP3 increase from 23 to 37 in the case of MP3-R30 and then begin to decrease as milling time increases (Table S2). This suggests that initially, Mg may have been leached out and later consumed in the formation of brucite, serpentine and carbonates during EW as the surface area increased. A similar trend can be observed in MP7. Moreover, magnesite, vaterite and siderite were found in MP7 residues (Fig. 10b; for carbonate details, refer to the supplementary information). The occurrence of magnesite in the untreated MP3 and MP7 samples can be attributed to natural carbonate formations within the Muslim Bagh Ophiolite via natural CO_2 sequestration processes (Ullah et al. 2014). However, its absence in the experimental residues, which was replaced by calcite or aragonite, suggests that magnesite dissolution and calcite formation may occur under mildly alkaline conditions. The occurrence of siderite as the primary carbonate species in the MP7 residue implies either a higher reactivity of iron in this sample or the resilience of siderite against dissolution under mildly alkaline conditions.

5 Summary

This study investigated the effects of EW on milled ultramafic rocks (e.g., peridotite and amphibolite) from the Muslim Bagh Ophiolite, Pakistan, in laboratory experiments involving seawater and CO_2. The reactions led to the formation of brucite, serpentine and carbonates. Data showed that as the specific surface area of the milled powders increased, the Mg/Ca ratio in the experimental filtrates decreased. This suggests that the enhanced reaction rates led to more Mg leaching from the original rock, which was then consumed in forming secondary minerals through various reaction pathways. LOI and TGA data confirmed the formation of these minerals by reflecting their distinct decomposition temperatures. XRD analysis confirmed the presence of carbonates, while SEM images of the residues showed textural changes consistent with secondary minerals identified in the petrographic study of the original rock. Control experiments demonstrated a decrease in pH when seawater and CO_2 reacted, underlining the ocean acidification caused by increased CO_2 emissions. However, the experimental filtrates showed an increase in pH, indicating that peridotite and amphibolite powders can effectively raise the pH of seawater as a result of EW. This study also provides an analog for EW applications in various geological settings where Mg- and Ca-bearing ultramafic rocks interact with carbon-rich aqueous fluids, including coastal and open ocean environments. Taken together, EW of ultramafic powders in these environments appears viable for sequestering dissolved CO_2 and increasing ocean pH to mitigate climate change and ocean acidification. Further research is needed to explore the effects of other labile elements, such as silicon and iron, that may leach during the EW process. Additionally, more experiments under different pH and temperature conditions are required to optimize carbonate formation for effective CO_2 sequestration.

Acknowledgements The authors express gratitude for the editorial assistance provided by the editorial office . We acknowledge the anonymous reviewers for insightful feedback that added valuable discussion to the manuscript. The authors thank Khulood Alhinai for assistance in experimental setup during earlier stages of the study. The authors extend their gratitude to Myo Myint from the Department of Physics (SQU) for the SEM images, Dr. Salah Jellali from CESAR (SQU) for providing the TGA data, and acknowledge Qatar University for facilitating this research. The first author was supported by internal grant from Sultan Qaboos University (IG/DVC/ESRC/21/01).

Author's contribution AA contributed to conception and design of the study. AA wrote the first draft of the manuscript. MIR, ME, HUR, IAA and MM wrote sections of the manuscript. All authors contributed to manuscript revision, read and approved the submitted version.

Declarations

Conflict of interest The authors state that there is no conflict of interest. The funders played no part in research design, data collection, analysis, interpretation, manuscript writing or the decision to publish the results.

References

Ali A, Abbasi IA, Nogueira LB, Hersi OS, Al Kindi SAN, El-Ghali MAK, Nasir S (2021) Geochemical and C–O isotopic study of ophiolite-derived carbonates of the Barzaman Formation, Oman: Evidence of natural CO_2 sequestration via carbonation of ultramafic clasts. J Geophys Res Solid Earth 126:e2020JB021290. https://doi.org/10.1029/2020JB021290

Arjen, Luijendijk Gerben, Hagenaars Roshanka, Ranasinghe Fedor, Baart Gennadii, Donchyts Stefan, Aarninkhof (2018) The State of the World's Beaches Abstract Scientific Reports 8(1) https://doi.org/10.1038/s41598-018-24630-6

Balthasar U, Cusack M (2015) Aragonite-calcite seas-quantifying the gray area. Geology 43(2):99–102. https://doi.org/10.1130/G36293.1

Beerling DJ, Leake JR, Long SP, Scholes JD, Ton J, Nelson PN, Bird M, Kantzas E, Taylor LL, Sarkar B, Kelland M, DeLucia E, Kantola I, Müller C, Rau G, Hansen J (2018) Farming with crops and rocks to address global climate, food and soil security. Nat Plants 4:138–147. https://doi.org/10.1038/s41477-018-0108-y

Beerling DJ, Kantzas EP, Lomas MR, Wade P, Eufrasio RM, Renforth P, Sarkar B, Andrews MG, James RH, Pearce CR (2020) Potential for large-scale CO_2 removal via enhanced rock weathering with croplands. Nature 583:242–248. https://doi.org/10.1038/s41586-020-2448-9

Betts RA, Belcher SE, Hermanson L, Tank AK, Lowe JA, Jones CD, Morice CP, Rayner NA, Scaife AA, Stott PA (2023) Approaching 1.5 °C: How will we know we've reached this crucial warming mark? Nature 624:33–35.

Dietzen C, Harrison R, Michelsen-Correa S (2018) Effectiveness of enhanced mineral weathering as a carbon sequestration tool and alternative to agricultural lime: an incubation experiment. Int J Greenh Gas Control 74:251–258. https://doi.org/10.1016/j.ijggc.2018.05.007

Doney SC, Fabry VJ, Feely RA, Kleypas JA (2009) Ocean acidification: the other CO_2 problem. Ann Rev Mar Sci 1:169–192. https://doi.org/10.1146/annurev.marine.010908.163834

Fawzy S, Osman AI, Doran J, Rooney DW (2020) Strategies for mitigation of climate change: a review. Environ Chem Lett 18:2069–2094. https://doi.org/10.1007/s10311-020-01059-w

Friedlingstein P, O'Sullivan M, Jones MW, Andrew RM, Bakker DCE, Hauck J, Landschützer P, Le Quéré C, Luijkx IT, Peters GP, Peters W, Pongratz J, Schwingshackl C, Sitch S, Canadell JG, Ciais P, Jackson RB, Alin SR, Anthoni P, Barbero L, Bates NR, Becker M, Bellouin N, Decharme B, Bopp L, Brasika IBM, Cadule P, Chamberlain MA, Chandra N, Chau T-T-T, Chevallier F, Chini LP, Cronin M, Dou X, Enyo K, Evans W, Falk S, Feely RA, Feng L, Ford DJ, Gasser T, Ghattas J, Gkritzalis T, Grassi G, Gregor L, Gruber N, Gürses Ö, Harris I, Hefner M, Heinke J, Houghton RA, Hurtt GC, Iida Y, Ilyina T, Jacobson AR, Jain A, Jarníková T, Jersild A, Jiang F, Jin Z, Joos F, Kato E, Keeling RF, Kennedy D, Klein Goldewijk K, Knauer J, Korsbakken JI, Körtzinger A, Lan X, Lefèvre N, Li H, Liu J, Liu Z, Ma L, Marland G, Mayot N, McGuire PC, McKinley GA, Meyer G, Morgan EJ, Munro DR, Nakaoka S-I, Niwa Y, O'Brien KM, Olsen A, Omar AM, Ono T, Paulsen M, Pierrot D, Pocock K, Poulter B, Powis CM, Rehder G, Resplandy L, Robertson E, Rödenbeck C, Rosan TM, Schwinger J, Séférian R, Smallman TL, Smith SM, Sospedra-Alfonso R, Sun Q, Sutton AJ, Sweeney C, Takao S, Tans PP, Tian H, Tilbrook B, Tsujino H, Tubiello F, van der Werf GR, van Ooijen E, Wanninkhof R, Watanabe M, Wimart-Rousseau C, Yang D, Yang X, Yuan W, Yue X, Zaehle S, Zeng J, Zheng B (2023) Global carbon budget 2023. Earth System Sci Data 15:5301–5369. https://doi.org/10.5194/essd-15-5301-2023

Fuss S, Lamb WF, Callaghan MW, Hilaire J, Creutzig F, Amann T, Beringer T, de Oliveira GW, Hartmann J, Khanna T (2018) Negative emissions—part 2: costs, potentials and side effects. Environ Res Lett 13:063002. https://doi.org/10.1088/1748-9326/aabf9f

Haywood HM, Eyre JM, Scholes H (2001) Carbon dioxide sequestration as stable carbonate minerals—environmental barriers. Env Geol 41:11–16.

Huag AH, Kleiv RA, Munz IA (2010) Investigating dissolution of mechanically activated olivine for carbonation purposes. Appl Geochem 25:1547–1563. https://doi.org/10.1016/j.apgeochem.2010.08.005

Gattuso J-P, Hansson L (eds) (2011) Ocean acidification, Oxford University Press.

Gattuso JP, Magnan A, Billé R, Cheung WWL, Howes EL, Joos F, Allemand D, Bopp L, Cooley SR, Eakin CM, Hoegh-Guldberg O, Kelly RP, Pörtner H-O, Rogers AD, Baxter JM, Laffoley D, Osborn D, Rankovic A, Rochette J, Sumaila UR, Treyer S, Turley C (2015) Contrasting futures for ocean and society from different anthropogenic CO2 emissions scenarios. Science 349:aac4722. https://doi.org/10.1126/science.aac4722

Gerdemann SJ, Dahlin DC, O'Connor WK (2002) Carbon dioxide sequestration by aqueous mineral carbonation of magnesium silicate minerals. DOE/ARC-2003–018.

Gerdemann SJ, O'Connor WK, Dahlin DC, Penner LR, Rush H (2007) *Ex situ* aqueous mineral carbonation. Env Sci Tech 41:2587–2593.

Goff F, Lackner KS (1998) Carbon dioxide sequestering using ultramafic rocks. Env Geosci 5(3):89–101.

Gruber N, Clement D, Carter BR, Feely RA, Van Heuven S, Hoppema M, Ishii M, Key RM, Kozyr A, Lauvset SK, Lo Monaco C, Mathis JT, Murata A, Olsen A, Perez FF, Sabine CL, Tanhua T, Wanninkhof R (2019) The oceanic sink for anthropogenic CO_2 from 1994 to 2007. Science 363(6432):1193–1199. https://doi.org/10.1126/science.aau5153

Hartmann J, West AJ, Renforth P, Köhler P, De La Rocha CL, Wolf-Gladrow DA, Dürr HH, Scheffran J (2013) Enhanced chemical weathering as a geoengineering strategy to reduce atmospheric carbon dioxide, supply nutrients, and mitigate ocean acidification. Rev Geophys 51:113–149. https://doi.org/10.1002/rog.20004

Huijgen WJJ, Ruijg GJ, Comans RNJ, Witkamp GJ (2006) Energy consumption and net CO_2 sequestration of aqueous mineral carbonation. Ind Eng Chem Res 45:9184–9194.

IPCC (2021) Climate change 2021: The physical science basis. contribution of working group I to the sixth assessment report of the intergovernmental panel on climate change. In: Masson-Delmotte V, Zhai P, Pirani A, Connors SL, Péan C, Berger S, Caud N, Chen Y, Goldfarb L, Gomis MI, Huang M, Leitzell K, Lonnoy E, Matthews JBR, Maycock TK, Waterfield T, YelekçI O, Yu R, Zhou B (eds) Cambridge University Press, Cambridge.

Jia L, Anthony EJ, Gale J, Kaya Y (eds) (2002) Proceedings of 6th International Conference on greenhouse gas control technologies (GHGT-6), Kyoto, Japan.

Kojima T, Nagamine A, Uene N, Uemiya S (1997) Absorption and fixation of carbon dioxide by rock weathering. Energy Con Man 38:S461–S466

Kakizawa M, Yamasaki A, Yanagisawa Y (2001) A new CO_2 disposal process using artificial rock weathering of calcium silicate by acetic acid. Energy 26(4):341–354.

Kantzas EP, Val Martin M, Lomas MR, Eufrasio RM, Renforth P, Lewis AL, Taylor LL, Mecure J-F, Pollitt H, Vercoulen PV, Vakilifard N, Holden PB, Edwards NR, Koh L, Pidgeon NF, Banwart SA, Beerling DJ (2022) Substantial carbon drawdown potential from enhanced rock weathering in the United Kingdom. Nat Geosci 15:382–389. https://doi.org/10.1038/s41561-022-00925-2

Kakar MI, Khan M, Mahmood K, Kerr AC (2014) Facies and distribution of metamorphic rocks beneath the Muslim Bagh ophiolite, (NW Pakistan): Tectonic implications. J Himalayan Earth Sci 47(2):115.

Köhler P, Hartmann J, Wolf-Gladrow DA (2010) Geoengineering potential of artificially enhanced silicate weathering of olivine. Proc Natl Acad Sci USA 107:20228–20233. https://doi.org/10.1073/pnas.1000545107

Kelemen P, Matter JM (2008) *In situ* carbonation of peridotite for CO_2 storage. Proc Nat Acad Sci USA 105(45):17295–17300.

Lackner KS, Wendt CH, Butt DP, Joyce EL, Sharp DH (1995) Carbon dioxide disposal in carbonate minerals. Energy 20:1153–1170. https://doi.org/10.1016/0360-5442(95)00071-N

Le Quéré C, Moriarty R, Andrew RM, Canadell JG, Sitch S, Korsbakken JI, Friedlingstein P, Peters GP, Andres RJ, Boden TA, Houghton RA, House JI, Keeling RF, Tans P, Arneth A, Bakker DCE, Barbero L, Bopp L, Chang J, Chevallier F, Chini LP, Ciais P, Fader M, Feely RA, Gkritzalis T, Harris I, Hauck J, Ilyina T, Jain AK, Kato E, Kitidis V, Klein Goldewijk K, Koven C, Landschützer P, Lauvset SK, Lefèvre N, Lenton A, Lima ID, Metzl N, Millero F, Munro DR, Murata A, Nabel JEMS, Nakaoka S, Nojiri Y, O'Brien K, Olsen A, Ono T, Pérez FF, Pfeil B, Pierrot D, Poulter B, Rehder G, Rödenbeck C, Saito S, Schuster U, Schwinger J, Séférian R, Steinhoff T, Stocker BD, Sutton AJ, Takahashi T, Tilbrook B, van der Laan-Luijkx IT, van der Werf GR, van Heuven S, Vandemark D, Viovy N, Wiltshire A, Zaehle S, Zeng N (2015) Global carbon budget 2015. Earth System Sci Data 7(2):349–396. https://doi.org/10.5194/essd-7-349-2015

Mark J., Mitchell Oliver E., Jensen K. Andrew, Cliffe M. Mercedes, Maroto-Valer (2010) A model of carbon dioxide dissolution and mineral carbonation kinetics Proceedings of the Royal Society A: Mathematical Physical and Engineering Sciences 466(2117): 1265–1290 https://doi.org/10.1098/rspa.2009.0349

Matter JM, Kelemen PB (2009) Permanent storage of carbon dioxide in geological reservoirs by mineral carbonation. Nat Geosci 2(12):837–841.

Matter JM, Stute M, Snæbjörnsdottir SO, Oelkers EH, Gislason SR, Aradottir ES, Sigfusson B, Gunnarsson I, Sigurdardottir H, Gunnlaugsson E, Axelsson G, Alfredsson HA, Wolff-Boenisch D, Mesfin K, Taya DFR, Hall J, Dideriksen K, Broecker WS (2016) Rapid carbon mineralization for permanent disposal of anthropogenic carbon dioxide emissions. Science 352(6291):1312–1314. https://doi.org/10.1126/science.aad8132

McGrail BP, Spane F, Sullivan E, Bacon D, Hund G (2011) The Wallula basalt sequestration pilot project. Energy Procedia 4:5653–5660. https://doi.org/10.1016/j.egypro.2011.02.557

McGrail BP, Spane FA, Amonette JE, Thompson C, Brown CF (2014) Injection and monitoring at the Wallula basalt pilot project. Energy Proc 63:2939–2948. https://doi.org/10.1016/j.egypro.2014.11.316

McGrail BP, Schaef HT, Spane FA, Cliff JB, Qafoku O, Horner JA, Thompson CJ, Owen AT, Sullivan CE (2017) Field validation of supercritical CO_2 reactivity with basalts. Environ Sci Technol Lett 4(1):6–10. https://doi.org/10.1021/acs.estlett.6b00387

Mentaschi L, Vousdoukas MI, Pekel J-F, Voukouvalas E, Feyen L (2018) Global long-term observations of coastal erosion and accretion. Sci Rep 8(1):1–11.

Montserrat F, Renforth P, Hartmann J, Leermakers M, Knops P, Meysman FJR (2017) Olivine dissolution in seawater: Implications for CO_2 sequestration through enhanced weathering in coastal environments. Environ Sci Technol 51:3960–3972. https://doi.org/10.1021/acs.est.6b05942

Nicolas A, Boudier E, Ildefonse B, Bal E (2000) Accretion of Oman and United Arab Emirates ophiolite: Discussion of a new structural map. Mar Geophys Res 21(3–4):147–179.

O'Connor WK, Dahlin CL, Nilsen DN, Rush GE, Walters RP, Turner PC (2000) CO_2 storage in solid form: A study of direct mineral carbonation. DOE/ARC-2000–011.

O'Connor WK, Dahlin DC, Rush GE, Gerdemann SJ, Penner LR, Nilsen DN (2005) Aqueous mineral carbonation: mineral availability, pretreatment, reaction parametrics, and process studies. DOE/ARC-TR-04–002. https://doi.org/10.13140/RG.2.2.23658.31684

Orr JC, Fabry VJ, Aumont O, Bopp L, Doney SC, Feely RA, Gnanadesikan A, Gruber N, Joos F, Key RM, Lindsay K, Maier-Reimer E, Matear R, Monfray P, Mouchet A, Najjar RG, Plattner G, Rodgers KB, Sabine CL, Sarmiento JL, Schlitzer R, Slater RD, Totterdell IJ, Weirig M, Yamanaka Y, Yool A (2005) Anthropogenic ocean acidification over the twenty-first century and its impact on calcifying organisms. Nature 437:681–686. https://doi.org/10.1038/nature04095

Pilkey OH, Cooper JAG (2004) Society and sea level rise. Science 303:1781–1781.

Renforth P, Pogge von Strandmann PAE, Henderson GM (2015) The dissolution of olivine added to soil: Implications for enhanced weathering. Appl Geochem 61:109–118. https://doi.org/10.1016/j.apgeochem.2015.05.016

Riebesell U, Czerny J, von Bröckel K, Boxhammer T, Büdenbender J, Deckelnick M, Fischer M, Hoffmann D, Krug SA, Lentz U, Ludwig A, Muche R, Schulz KG (2013) A mobile sea-going mesocosm system–new opportunities for ocean change research. Biogeosciences 10(3):1835–1847. https://doi.org/10.5194/bg-10-1835-2013

Rigopoulos I, Harrison AL, Delimitis A, Ioannou I, Efstathiou AM, Kyratsi T, Oelkers EH (2018) Carbon sequestration via enhanced weathering of peridotites and basalts in seawater. Appl Geochem 91:197–207. https://doi.org/10.1016/j.apgeochem.2017.11.001

Sanna A, Uibu M, Caramanna G, Kuusik R, Maroto-Valera MM (2014) A review of mineral carbonation technologies to sequester CO_2. Chem Soc Rev 43:8049–8080. https://doi.org/10.1039/C4CS00035H

Schuiling RD, Krijgsman P (2006) Enhanced weathering: an effective and cheap tool to sequester CO2. Clim Change 74:349–354. https://doi.org/10.1007/s10584-005-3485-y

Siva T, Muralidharan S, Sathiyanarayanan S, Manikandan E, Jayachandran M (2017) Enhanced polymer induced precipitation of polymorphous in calcium carbonate: Calcite aragonite vaterite phases. J Inorg Organomet Polym 27:770–778.

Streckeisen A (1976) To each plutonic rock its proper name. Earth Sci Rev 12:1–33.

Taylor LL, Quirk J, Thorley RMS, Kharecha PA, Hansen J, Ridgwell A, Lomas MR, Banwart SA, Beerling DJ (2016) Enhanced weathering strategies for stabilizing climate and averting ocean acidification. Nat Clim Change 6:402–406. https://doi.org/10.1038/nclimate2882

Tignor M, Allen S (2013) Fifth assessment report of the intergovernmental panel on climate change (IPCC). UK/New York, USA, Cambridge.

Tro NJ (2022) Chemistry: A molecular approach, 6th edn. Published by Pearson, Santa Barbara City College.

Turianicová E, Baláž P, Tuček L, Zorkovská A, Zeleňák V, Németh Z, Šatka A, Kováč J (2013) A comparison of the reactivity of activated and non-activated olivine with CO_2. Int J Min Process 123:73–74. https://doi.org/10.1016/j.minpro.2013.05.006

Ullah I (2014) Mode of occurrence and economic potential of magnesite deposits, Nisai area Muslim Bagh Balochistan Thesis.

UNFCCC (2015) Report of the Conference of the parties to the United Nations Framework Convention on Climate Change, 21st Session, 2015, Paris, Vol. 4, report no. FCCC/CP/2015/10.

U.S. EPA (1994) Method 200.7: Determination of Metals and Trace Elements in Water and Wastes by Inductively Coupled Plasma-Atomic Emission Spectrometry," Revision 4.4. Cincinnati, OH.

Viti C (2010) Serpentine minerals discrimination by thermal analysis. Am Miner 95:631–638.

Watson AJ, Schuster U, Shutler JD, Holding T, Ashton IG, Landschützer P, Woolf DK, Goddijn-Murphy L (2020) Revised estimates of ocean-atmosphere CO_2 flux are consistent with ocean carbon inventory. Nature Comm 11(1):1–6. https://doi.org/10.1038/s41467-020-18203-3

Zeebe R, Wolf-Gladrow D (2001) CO_2 in seawater: Equilibrium, kinetics. Isotopes Elsevier Oceanography Series 65:346.

Zhu W, Fusseis F, Lisabeth H, Xing T, Xiao X, De Andrade V, Karato S (2016) Experimental evidence of reaction-induced fracturing during olivine carbonation: fracturing during olivine carbonation. Geophys Res Lett https://doi.org/10.1002/2016GL070834